

Cell Discovery in Millimeter Wave Systems: Physical Layer Implementations

Rashmi P, Manoj A, Arun Pachai Kannu.

Abstract—Cell discovery is the procedure in which an user equipment (UE) in a cellular network finds a suitable base station (BS) and its physical layer cell identity, in order to establish a link-layer connection. When beamforming with antenna arrays is done at both transmitter and receiver, cell discovery in mm wave systems also involves finding the correct angle of arrival (AoA) - angle of departure (AoD) alignment between the UE and the detected BS. In this paper, we consider various existing and new schemes for cell discovery, present analytical studies on their detection probability and compare them in a common framework. In the first part, we study the conventional beam sweep technique and its variations, and present their physical layer training phase in detail. While the traditional beam sweep can not directly find the identity of the detected BS, we provide modifications in its training phase to enable the cell identity detection. In the second part of the paper, exploiting the sparseness of the mm wave channels and using an equivalent compressive sensing measurement model, we develop new cell discovery schemes with lesser overheads. One such design involves mutually unbiased bases (MUB) from quantum information theory. For the MUB based training scheme, we characterize the mutual coherence parameter of the resulting sensing matrix and establish its connection to the detection probability. We also present detailed simulation studies using experimentally driven mm wave channel simulators and show that our MUB based scheme gives superior performance compared to all the other schemes.

Index Terms—beam sweeping, detection probability, compressive sensing, mutually unbiased bases, random beamforming

I. INTRODUCTION

Millimeter Wave (mm wave) communication systems are viewed as a potential candidate for the 5G cellular technology, to meet the continuous increase in the volume of mobile data, the demand for high data rate services and to achieve large network coverage [1]–[3]. Beamforming is a key enabling technique in mm wave communications which compensates the high path losses of the mm waves, by employing highly directional signal transmission and reception with large antenna arrays. Cell discovery (CD) is a procedure by which an user equipment (UE) entering a network finds a suitable (nearby) base station (BS) and its identity, in order to establish a link layer connection. Directional signaling in mm wave systems makes the cell discovery process very challenging, when compared with the sub-6 GHz microwave systems.

User discovery is a dual problem of CD, where a BS tries to identify the presence of a UE intending to make a connection. Several studies have been done in the literature to address

cell or user discovery problem in mm wave systems. Beam sweeping is a conventional CD technique [4], [5], where both transmitter and receiver sweep their beams along the entire angular range (say, 360 degrees) and make a detection based on the angle of arrival (AoA) - angle of departure (AoD) beam-pair corresponding to the largest received signal strength. In general, beam sweeping incurs large training overhead, as all the beam-pair combinations need to be tried out before making a decision. In order to reduce the overhead of beam sweep, several variations have been proposed in the literature.

In [6], a detection algorithm with omni-directional transmission and directed reception is shown to have a better trade-off over the directional beam sweep in terms of received SNR versus detection delay. Beamforming using broadened beams was proposed in [7] and is verified to be superior than the traditional MUSIC and ESPRIT algorithms, which are commonly employed for AoA estimation in wireless communication. In [8]–[10], considering an environment with mm wave pico-cells assisted by a macro BS, new CD techniques were proposed which use context information such as the estimated user location. In [11], a similar approach is considered for the cell discovery problem. However, the performance of these schemes completely rely on the accuracy of the estimate on user position. In the iterative search algorithm proposed in [12], the BS scans its space sector-wise and when the BS speculates the existence of the UE in a particular sector, it partitions the identified sector into smaller sectors and scans them using narrower beams iteratively. In [13] a hybrid cell search method is proposed which combines the important aspects of the exhaustive search and the iterative search techniques.

With omni directional transmissions during CD [6], the communication range (distance) of the systems gets reduced and CD is possible only within this limited range. In addition, the omni directional CD procedure does not reveal the exact AoA-AoD alignment between the transmitter and receiver, which is needed during the data transmission phase to reap the beamforming gains of large antenna arrays. For the iterative CD techniques [12], [13], the feedback overhead from UE or BS during CD process scales with the number of UEs. In addition, BS has to adapt its transmission beams based on the UE feedback, which implies that the training process of each UE need to be carried out separately. In view of these issues, we focus on developing CD techniques which can identify the correct AoA-AoD alignment between the BS and UE, without using any feedback during the CD procedure.

In the first part of the work, we discuss the physical layer implementation details of the conventional beam sweep

Rashmi P (ee15d054@ee.iitm.ac.in), Manoj A (ee14d210@ee.iitm.ac.in) and Arun Pachai Kannu (arunpachai@ee.iitm.ac.in) are with Electrical Engineering Department, Indian Institute of Technology Madras, Chennai - 600036, India.

technique by completely specifying its training phase, with the explicit description of beamforming vectors to be used at the transmitter and receiver. We also discuss how the beamforming vectors can be modified to implement beam widening or beam combining variations. With the explicit characterization of the training phase, we find analytical expressions for the detection probability and false alarm probability of beam sweep and its variations, under certain assumptions on the mm wave channel models. While the conventional beam sweep technique can not find the identity of the detected BS, we propose new modifications in its training phase using differential encoding schemes to incorporate this capability.

In the second part of the work, by exploiting the sparse nature of mm wave channels [14], [15], we formulate CD problem as a sparse signal recovery problem in compressive sensing (CS) [16] and develop two new training schemes: 1) beamforming vectors are designed based on mutually unbiased bases (MUB) from quantum information theory [17] and 2) beamforming vectors are randomly generated. We obtain analytical expression for the cell detection probability of the new schemes. Mutual coherence parameter of the sensing matrix [18] plays a significant role in the sparse signal recovery performance [18], [19]. We characterize the mutual coherence for our MUB based beamforming (MUBB) scheme and establish its relation to the cell detection probability. Among all the schemes considered, our MUBB yields the smallest mutual coherence. We also perform simulation studies using NYUSIM [20], [21], an experimentally driven mm wave channel simulator and conclude that our MUBB is superior to other CD techniques, in terms of both training overhead and cell detection performance. Main contributions of our work are summarized as:

- Obtain analytical expressions for detection and false alarm probabilities for beam sweep and beam combining techniques.
- Propose differential encoding based beam sweep technique to find the identity of the detected BS.
- Propose two new training schemes, random beamforming and MUB based beamforming, with smaller overheads compared to the beam sweep technique. Obtain the analytical expression for the detection probability of the new schemes.
- Establish the superior performance of our MUBB over all the other schemes using simulation studies with NYUSIM.

Notations: Mathcal font \mathcal{P} denotes a set and its cardinality is $|\mathcal{P}|$. p and P denote scalars, \mathbf{p} - vector and \mathbf{P} - matrix. $[\mathbf{P}]_{p,\bar{p}}$ refers to the $(p,\bar{p})^{th}$ element of matrix \mathbf{P} and \mathbf{p}_p the p^{th} element of vector \mathbf{p} . Also, $\mathbf{P}_{\mathcal{P}}$ is a sub-matrix of \mathbf{P} whose columns are those of \mathbf{P} indexed by the set \mathcal{P} . Similarly, $\mathbf{p}_{\mathcal{P}}$ is a sub-vector of \mathbf{p} containing elements of \mathbf{p} indexed by \mathcal{P} . p^{th} row and p^{th} column of \mathbf{P} is denoted as $[\mathbf{P}]_{p,:}$ and $[\mathbf{P}]_{:,p}$ respectively. $[\mathbf{P}_1 | \mathbf{P}_2 | \dots | \mathbf{P}_P]$ denotes concatenation of matrices \mathbf{P}_1 to \mathbf{P}_P . \mathbf{I}_p and \mathbf{F}_p denote identity and unitary DFT matrices of size $p \times p$ each. $\mathbf{0}_p$ and $\mathbf{1}_p$ indicate an all-zero vector and all-one vector respectively, each of length p . Lastly, $\|\cdot\|_2$ is the l_2 -norm and $\mathbb{E}[\cdot]$ is the expectation operator.

$(\cdot)^*$ and $(\cdot)^T$ denote Hermitian and transpose respectively.

II. SYSTEM MODEL AND PROBLEM STATEMENT

Consider a mm wave network with N_{bs} base stations (BSs), each equipped with a uniform linear array of antennas (ULA) of size $N_t \times 1$. Assume that the user equipment (UE) has an ULA of size $N_r \times 1$. The channel from the i^{th} BS to the UE, denoted by \mathbf{H}_i (of size $N_r \times N_t$), is modeled as [2], [15], [22],

$$\mathbf{H}_i = \sum_{k=1}^{K_i} \alpha_k^{(i)} \mathbf{a}_{r_k}^{(i)} \left(\mathbf{a}_{t_k}^{(i)} \right)^*, \quad (1)$$

where K_i is the total number of multi-path components, $\alpha_k^{(i)}$ is the complex channel gain of the k^{th} multi-path and $\mathbf{a}_{r_k}^{(i)}$ and $\mathbf{a}_{t_k}^{(i)}$ are the corresponding transmit and receive antenna array response vectors. The array response vectors depend on the AoA and AoD of the corresponding multi-path. Specifically, $\mathbf{a}_{r_k}^{(i)} = \frac{1}{\sqrt{N_r}} [1 e^{-j\omega_{r_k}^{(i)}} \dots e^{-j(N_r-1)\omega_{r_k}^{(i)}}]^T$ and $\mathbf{a}_{t_k}^{(i)} = \frac{1}{\sqrt{N_t}} [1 e^{-j\omega_{t_k}^{(i)}} \dots e^{-j(N_t-1)\omega_{t_k}^{(i)}}]^T$, where $\omega_{r_k}^{(i)} = 2\pi \frac{d}{\lambda} \sin(\theta_{r_k}^{(i)})$ and $\omega_{t_k}^{(i)} = 2\pi \frac{d}{\lambda} \sin(\theta_{t_k}^{(i)})$, d is the inter-element spacing between adjacent antennas in the ULA (at both the BSs and the UE), λ is the operating carrier wavelength, and $\theta_{r_k}^{(i)}$ and $\theta_{t_k}^{(i)}$ are the AoA and AoD respectively, associated with the k^{th} multi-path component of the channel \mathbf{H}_i . The channel gains, $\alpha_k^{(i)}$'s, are distributed as independent $\mathcal{CN}(0, \sigma_{k_i}^2)$. Note that, when a given BS is blocked or far away from the UE, the corresponding multi-path gains will be close to zero.

Each AoA-AoD pair $(\theta_{r_k}^{(i)}, \theta_{t_k}^{(i)})$ leads to a spatial frequency pair $(\omega_{r_k}^{(i)}, \omega_{t_k}^{(i)})$ so that the 2D Fourier transform of \mathbf{H}_i will have significant energies in the DFT bins closer to $(\omega_{r_k}^{(i)}, \omega_{t_k}^{(i)})$. Since the number of multi-paths is small compared to the array sizes, the mm wave channels are approximately sparse in Fourier basis [14], [15], [22]. Specifically, 2D Fourier transform of \mathbf{H}_i , computed using unitary DFT matrices as,

$$\mathbf{G}_i = \mathbf{F}_{N_r}^* \mathbf{H}_i \mathbf{F}_{N_t}, \quad (2)$$

is an approximately sparse matrix. The locations of significant valued entries in \mathbf{G}_i provide indication of the AoA-AoD pairs corresponding to the strong paths between UE and i^{th} BS. On the other hand, under *ideal channel conditions*, when the spatial frequencies fall exactly on the DFT bins,

$$\omega_{r_k}^{(i)} \in \left\{ \frac{2\pi l}{N_r}, l = 0, \dots, N_r - 1 \right\}, \forall k, \quad (3)$$

$$\omega_{t_k}^{(i)} \in \left\{ \frac{2\pi m}{N_t}, m = 0, \dots, N_t - 1 \right\}, \forall k, \quad (4)$$

the matrix \mathbf{G}_i is an *exactly* sparse matrix with K_i independent Gaussian non-zero entries in the DFT bins given by the spatial frequency pairs $(\omega_{r_k}^{(i)}, \omega_{t_k}^{(i)})$.

Suppose i^{th} BS transmits data symbol x_i using a beamforming vector \mathbf{w}_{t_i} , then the received signal at the UE y is given by,

$$y = \mathbf{w}_r^* \left(\sum_{i=1}^{N_{bs}} \mathbf{H}_i \mathbf{w}_{t_i} x_i \right) + \underbrace{\mathbf{w}_r^* \mathbf{n}}_n, \quad (5)$$

where \mathbf{w}_r is the receive beamforming vector and \mathbf{n} is the additive N_r -length noise vector. We assume, $\mathbf{n} \sim \mathcal{CN}(\mathbf{0}, \sigma_n^2 \mathbf{I}_{N_r})$ and hence $n \sim \mathcal{CN}(0, \sigma_n^2 \|\mathbf{w}_r\|_2^2)$. For convenience and consistency, we always set the receive beamforming vector to be of unit norm, which yields $n \sim \mathcal{CN}(0, \sigma_n^2)$.

In this paper, we consider the cell discovery in mm wave systems where a UE endeavors to detect the presence of at least one accessible BS to establish a communication link. For this purpose, we consider the training phase where BSs and UE use known/fixed set of beamforming vectors and transmit known set of symbols. UE has a set of P beamforming vectors $\{\mathbf{w}_r^{(1)}, \dots, \mathbf{w}_r^{(P)}\}$ and each BS has a set of Q beamforming vectors $\{\mathbf{w}_{t_i}^{(1)}, \dots, \mathbf{w}_{t_i}^{(Q)}\}$. The received observation corresponding to a given transmit/receive beamforming vectors pair is

$$y_{p,q} = \mathbf{w}_r^{(p)*} \left(\sum_{i=1}^{N_{\text{bs}}} \mathbf{H}_i \mathbf{w}_{t_i}^{(q)} x_{p,q}^{(i)} \right) + n_{p,q}, \quad (6)$$

$$= \mathbf{w}_r^{(p)*} \left(\sum_{i=1}^{N_{\text{bs}}} \mathbf{F}_{N_r} \mathbf{G}_i \mathbf{F}_{N_t}^* \mathbf{w}_{t_i}^{(q)} x_{p,q}^{(i)} \right) + n_{p,q}, \quad (7)$$

where $x_{p,q}^{(i)}$ are the known transmit symbols and $\{n_{p,q}\}$ are i.i.d. complex Gaussian noise samples with variance σ_n^2 . We assume that all the pilot symbols transmitted have equal power, $|x_{p,q}^{(i)}|^2 = \rho, \forall p, q, i$. If all the combinations of transmit/receive beamforming pairs are used, then the training phase duration will be $M = PQ$. Using these M training phase observations in (7), we solve the CD problem by finding the locations of significant valued entries in the Fourier domain channel matrices $\{\mathbf{G}_i\}$. This leads to finding a suitable BS of sufficient signal strength and the corresponding AoA-AoD alignment. Different choices for beamforming vectors in the training phase lead to different CD techniques.

III. BEAM SWEEP TECHNIQUES AND VARIATIONS

In this section, we discuss a pilot training scheme called *beam sweep* (B-S) which is based on the conventional beamforming training technique used in traditional MIMO systems [4], [5]. In this method, the transmitter and receiver exhaustively search the optimal AoA-AoD pair, by sweeping their beams in the entire $[0, 2\pi]$ space and using all the transmit/receive beam combinations.

A. Conventional Beam Sweep:

In this scheme, the beamforming vectors $\{\mathbf{w}_{t_i}^{(q)}\}_{q=1}^Q$ and $\{\mathbf{w}_r^{(p)}\}_{p=1}^P, \forall i = 1, \dots, N_{\text{bs}}$ are chosen as columns of the unitary DFT matrices \mathbf{F}_{N_t} and \mathbf{F}_{N_r} respectively. Setting $P = N_r$ and $Q = N_t$, we have,

$$\mathbf{w}_{t_i}^{(q)} = [\mathbf{F}_{N_t}]_{:,q}, \quad q \in \{1, \dots, N_t\}, \forall i = 1, \dots, N_{\text{bs}}, \quad (8)$$

$$\mathbf{w}_r^{(p)} = [\mathbf{F}_{N_r}]_{:,p}, \quad p \in \{1, \dots, N_r\}. \quad (9)$$

Note that, when a beamforming vector is set as a column of a DFT matrix, the signal radiated by the antenna array is directed at an angle corresponding to the (spatial) frequency

given by that column. In the conventional B-S, we perform exhaustive search by considering all the transmit/receive beam combinations, leading to a total of $M = N_t N_r$ measurements, which are given by,

$$\begin{aligned} y_{p,q} &= [\mathbf{F}_{N_r}]_{:,p}^* \sum_{i=1}^{N_{\text{bs}}} \mathbf{F}_{N_r} \mathbf{G}_i \mathbf{F}_{N_t}^* [\mathbf{F}_{N_t}]_{:,q} x_{p,q}^{(i)} + n_{p,q} \\ &= \sum_{i=1}^{N_{\text{bs}}} x_{p,q}^{(i)} [\mathbf{G}_i]_{p,q} + n_{p,q}, \end{aligned} \quad (10)$$

with $p \in \{1, \dots, N_r\}$, $q \in \{1, \dots, N_t\}$. As mentioned earlier, the matrices $\{\mathbf{G}_i\}_{i=1}^{N_{\text{bs}}}$ are approximately sparse. For each $i = 1, \dots, N_{\text{bs}}$, we define the support set of \mathbf{G}_i , denoted as \mathcal{S}_i , as,

$$\mathcal{S}_i = \left\{ (a, b) \mid |[\mathbf{G}_i]_{a,b}|^2 > \delta, a = 1, \dots, N_r; b = 1, \dots, N_t \right\}, \quad (11)$$

where δ is an appropriately chosen limit value that declares whether or not an entry in matrix \mathbf{G}_i has considerably large magnitude. We define the support set $\mathcal{S} = \bigcup_{i=1}^{N_{\text{bs}}} \mathcal{S}_i$. For $(p, q) \in \mathcal{S}$, the received symbols $y_{p,q}$ in (10), have significant signal component due to sufficiently large channel gains and we term them as *active symbols*. For $(p, q) \notin \mathcal{S}$, the channel gains are close to zero and the corresponding observations are noise dominated. Now, detecting the presence of at least one accessible BS is equivalent to verifying whether there exists at least one active symbol among $\{y_{p,q}, p \in \{1, \dots, N_r\}, q \in \{1, \dots, N_t\}\}$. The active symbols $y_{p,q}$ are detected as

$$|y_{p,q}|^2 > \tau, \quad (12)$$

where τ is an appropriately chosen threshold. The indices (p, q) corresponding to the active symbols indicate the AoA-AoD alignment between the active BSs and UE. However, it does not reveal which BS among $i = 1, \dots, N_{\text{bs}}$ are active, since the observation is superposition of channel gains from all the BSs (10). Later in Section III-C, we discuss how differential encoding can be done using $x_{p,q}^{(i)}$, to enable finding the BS identity as well, using the observations $\{y_{p,q}\}$. For the above detection rule (12), the probability of false alarm \mathbb{P}_F and the probability of successful detection \mathbb{P}_D are given by

$$\begin{aligned} \mathbb{P}_F &= \mathbb{P} \left(\bigcup_{(p,q) \notin \mathcal{S}} |y_{p,q}|^2 > \tau \right) \\ &= \mathbb{P} \left(\max_{(p,q) \notin \mathcal{S}} |y_{p,q}|^2 > \tau \right), \end{aligned} \quad (13)$$

$$\mathbb{P}_D = \mathbb{P} \left(\bigcup_{(p,q) \in \mathcal{S}} |y_{p,q}|^2 > \tau \right). \quad (14)$$

Theorem 1. *For the conventional beam sweep technique with the detector (12), under the idealized channel conditions given in (3) and (4), the probability of false alarm is given by*

$$\mathbb{P}_F = 1 - \left(1 - e^{-\frac{\tau}{\sigma_n^2}} \right)^{N_t N_r - |\mathcal{S}|}. \quad (15)$$

For the same detector, with $|x_{p,q}^{(i)}|^2 = \rho$, the probability of successful detection \mathbb{P}_D is characterized as follows.

- **Non-overlap case:** When the support sets \mathcal{S}_i are disjoint

$$\bigcap_{i=1}^{N_{bs}} \mathcal{S}_i = \emptyset, \text{ we have}$$

$$\mathbb{P}_D = 1 - \prod_{i=1}^{N_{bs}} \prod_{k=1}^{K_i} \left[1 - \exp\left(-\frac{\tau}{\sigma_n^2 + \rho\sigma_{k_i}^2}\right) \right]. \quad (16)$$

- **Overlap case:** If $\bigcap_{i=1}^{N_{bs}} \mathcal{S}_i \neq \emptyset$, then \mathbb{P}_D can be lower bounded as,

$$\mathbb{P}_D \geq \exp\left(-\frac{\tau}{\sigma_n^2 + \rho \left[\max_{1 \leq i \leq N_{bs}} \max_{1 \leq k \leq K_i} \{\sigma_{k_i}^2\} \right]}\right). \quad (17)$$

Proof: Refer to Appendix A. ■

In both cases, asymptotically as $\sigma_n^2 \rightarrow 0$, $\mathbb{P}_D \rightarrow 1$.

B. Beam Combining method:

We present the details of beam combining (BC) or beam widening technique, where we widen (by combining multiple beams) the beams used during the training phase, so that the overall duration to sweep the entire angular space is reduced.

A direct approach to widen the beams for scanning the space is to employ training beamforming vectors that are constructed as (weighted) linear combination of the columns of \mathbf{F}_{N_t} and \mathbf{F}_{N_r} matrices at the BSs and UE respectively. Suppose, we combine β_t beams at the transmitter and β_r beams at the receiver, we need $P = \frac{N_r}{\beta_r}$ (widened) beams at the receiver and $Q = \frac{N_t}{\beta_t}$ (widened) beams at the transmitter. By using all the beam pair combinations, the total number of measurements needed is $M = \frac{N_t N_r}{\beta_t \beta_r}$. Compared to the B-S method, BC has reduced the training overhead by a factor of $\beta_t \beta_r$.

Now, we analyze the detection and false alarm performance of the BC method. To start with, we design the training phase beamforming vectors as,

$$\mathbf{w}_r^{(p)} = \frac{\sum_{l_r=1}^{\beta_r} [\mathbf{F}_{N_r}]_{:, (p-1)\beta_r + l_r}}{\sqrt{\beta_r}}, p = 1, \dots, \frac{N_r}{\beta_r}, \quad (18)$$

$$\mathbf{w}_{t_i}^{(q)} = \sqrt{\beta_r} \sum_{l_t=1}^{\beta_t} [\mathbf{F}_{N_t}]_{:, (q-1)\beta_t + l_t}, q = 1, \dots, \frac{N_t}{\beta_t} \quad (19)$$

with $i = 1, \dots, N_{bs}$. The normalization factor in (18) ensures that receive beamforming vectors are of unit norm, $\|\mathbf{w}_r^{(p)}\|_2^2 = 1, \forall p$. Because of the scaling factor in (19), we have $\|\mathbf{w}_{t_i}^{(q)}\|_2^2 = \beta_t \beta_r$. Now, the total squared norm (power) of the transmit beamforming vectors used at every BS for the entire training phase is $PQ\beta_t\beta_r = N_t N_r$, which is same as the total power of transmit beamforming vectors of the B-S method. This ensures some fairness in performance comparison, as the total power spent by both schemes for the training phase are identical, even though the training overheads are different.

The design of beamforming vectors proposed in equation

(19) results in the following,

$$\begin{aligned} \mathbf{F}_{N_t}^* \mathbf{w}_{t_i}^{(q)} &= \mathbf{F}_{N_t}^* \sum_{l_t=1}^{\beta_t} \sqrt{\beta_r} [\mathbf{F}_{N_t}]_{:, (q-1)\beta_t + l_t} \\ &= \sqrt{\beta_r} [\mathbf{I}_{N_t}^{(q)} \otimes \mathbf{1}_{\beta_t}], \end{aligned}$$

where $\mathbf{1}_k$ represents an all one column vector of size $k \times 1$ and $\mathbf{I}_k(p)$ is the p^{th} column of a $k \times k$ Identity matrix. Similarly, we have

$$\mathbf{w}_r^{(p)*} \mathbf{F}_{N_r} = \frac{[\mathbf{I}_{N_r}^{(p)} \otimes \mathbf{1}_{\beta_r}]^T}{\sqrt{\beta_r}}. \quad (20)$$

Based on these identities, the expression for the received symbols is given by,

$$y_{p,q} = \sum_{i=1}^{N_{bs}} \sum_{l_t=1}^{\beta_t} \sum_{l_r=1}^{\beta_r} x_{p,q}^{(i)} [\mathbf{G}_i]_{(p-1)\beta_r + l_r, (q-1)\beta_t + l_t} + n_{p,q}, \quad (21)$$

for $p = 1, \dots, \frac{N_r}{\beta_r}$ and $q = 1, \dots, \frac{N_t}{\beta_t}$. Intuitively, because of the widened beams used at both the BSs and UE, multiple DFT bins get mapped to the same scalar measurement at the UE. Equation (21) reveals this fact as the sum of all the elements of a $\beta_r \times \beta_t$ sub-matrix of \mathbf{G}_i (the elements are indicated by the two inner summations), contributes to the same measurement $y_{p,q}$ at the UE. Here, the active set $\mathcal{S}_{\text{actv}}$ is the set of indices $\{(p, q)\}$ for which the corresponding observation $y_{p,q}$ in (21) has contribution from at least one non-zero channel gain from any one of the support sets \mathcal{S}_i in (11). We employ the same thresholding rule (12) to detect the active set. Again, under ideal channel conditions (3),(4), false alarm probability for the BC scheme is

$$\mathbb{P}_F = 1 - \left(1 - e^{-\frac{\tau}{\sigma_n^2}}\right)^{\frac{N_t N_r}{\beta_t \beta_r} - |\mathcal{S}_{\text{actv}}|}, \quad (22)$$

The detection probability of BC scheme satisfies the same bound as given in (17). The derivations can be done in the same manner as Theorem 1.

C. Differential Encoding based Beam Sweep:

We noted that the detector in the conventional beam sweep (12) can not find the identity $i \in \{1, \dots, N_{bs}\}$ of the BS associated with the detected AoA-AoD alignment pair. Now, we propose modifications in the conventional beam sweep to enable the cell identity detection. Towards that, we obtain *two* sets of $M = N_t N_r$ measurements so that the total number of measurements is $2N_t N_r$. First set of $N_t N_r$ observations, denoted by $y_{p,q}$, is obtained as in the conventional beam sweep (10) by setting $x_{p,q}^{(i)} = 1, \forall p, q, i$. Second set of $N_t N_r$ observations, denoted by $\tilde{y}_{p,q}$, is obtained as in the conventional beam sweep (10) by setting $x_{p,q}^{(i)} = e^{j \frac{2\pi i}{(N_{bs}+1)}}$, $i = 1, \dots, N_{bs}$. Note that, during the second phase, each BS transmits a different constellation point from $(N_{bs} + 1)$ -ary PSK constellation. We have,

$$\tilde{y}_{p,q} = \sum_{i=1}^{N_{bs}} e^{j \frac{2\pi i}{(N_{bs}+1)}} [\mathbf{G}_i]_{p,q} + \tilde{n}_{p,q}. \quad (23)$$

Comparing (10) and (23), we note that the BS identity information is differentially encoded between the two sets of observations. In the detection phase, we first identify the set of active symbols as $\mathcal{S}_d = \left\{ (p, q) \mid (|y_{p,q}| + |\tilde{y}_{p,q}|)^2 > \tau \right\}$, where τ is an appropriately chosen threshold. If $\mathcal{S}_d = \emptyset$, then it means that the UE cannot recognize presence of any of the BSs. On the other hand, if $\mathcal{S}_d \neq \emptyset$, then for each of the detected AoA-AoD alignment $(p, q) \in \mathcal{S}_d$, the UE identifies the corresponding BS by performing the differential detection as

$$\hat{i}_{p,q} = \arg \min_{i \in \{1, \dots, N_{\text{bs}}\}} \left| \arg \left(\tilde{y}_{p,q} y_{p,q}^* \right) - \arg \left(e^{j \frac{2\pi i}{N_{\text{bs}}+1}} \right) \right|. \quad (24)$$

We also note that, this differential encoding can be incorporated in a straight forward manner with beam combining method as well.

IV. COMPRESSIVE SENSING BASED CELL DISCOVERY

A. Compressive Sensing Model:

As we mentioned in the system model, the Fourier domain channel matrices $\{\mathbf{G}_i\}$ are approximately sparse. Exploiting this sparseness, we develop an equivalent compressive sensing measurement model and formulate the CD problem as a sparse signal recovery problem. Towards that, we construct a $P \times Q$ measurement matrix \mathbf{Y} by stacking the observations $y_{p,q}$ in (6) as $[\mathbf{Y}]_{p,q} = y_{p,q}$. Setting $x_{p,q}^{(i)} = x$, $\forall p, q, i$, we have

$$\mathbf{Y} = \sum_{i=1}^{N_{\text{bs}}} \mathbf{W}_r^* \mathbf{H}_i \mathbf{W}_{t_i} x + \mathbf{N} \quad (25)$$

where $\mathbf{W}_{t_i} = [\mathbf{w}_{t_i}^{(1)} \ \mathbf{w}_{t_i}^{(2)} \ \dots \ \mathbf{w}_{t_i}^{(Q)}]$ for each i and $\mathbf{W}_r = [\mathbf{w}_r^{(1)} \ \mathbf{w}_r^{(2)} \ \dots \ \mathbf{w}_r^{(P)}]$. Here, we assume $|x|^2 = \rho$. Now, by vectorizing the matrices (by column-wise concatenation) $\mathbf{y} = \text{vec}(\mathbf{Y})$, $\mathbf{n} = \text{vec}(\mathbf{N})$, $\mathbf{h}^{(i)} = \text{vec}(\mathbf{H}_i)$, $\forall i$, $\mathbf{h} = [\mathbf{h}^{(1)T} \ \mathbf{h}^{(2)T} \ \dots \ \mathbf{h}^{(N_{\text{bs}})T}]^T$, we have

$$\mathbf{y} = \sum_{i=1}^{N_{\text{bs}}} \left(\mathbf{W}_{t_i}^T \otimes \mathbf{W}_r^* \right) \mathbf{h}^{(i)} x + \mathbf{n} = \mathbf{A} \mathbf{h} + \mathbf{n}, \quad (26)$$

with $\mathbf{A} = \left[\mathbf{W}_{t_1}^T \otimes \mathbf{W}_r^* \mid \mathbf{W}_{t_2}^T \otimes \mathbf{W}_r^* \mid \dots \mid \mathbf{W}_{t_{N_{\text{bs}}}}^T \otimes \mathbf{W}_r^* \right]$. The sparse representation of the mm wave channel matrices can be written as,

$$\mathbf{H}_i = \mathbf{F}_{N_r} \mathbf{G}_i \mathbf{F}_{N_t}^* \Rightarrow \mathbf{h}^{(i)} = \left(\mathbf{F}_{N_t}^* \otimes \mathbf{F}_{N_r} \right) \mathbf{g}^{(i)}, \forall i,$$

where $\mathbf{g}^{(i)} = \text{vec}(\mathbf{G}_i)$. Define $\mathbf{F} = \left(\mathbf{F}_{N_t}^* \right)^T \otimes \mathbf{F}_{N_r}$ and $\Phi = \mathbf{I}_{N_{\text{bs}}} \otimes \mathbf{F}$. Thus, $\mathbf{h} = \Phi \mathbf{g}$, where $\mathbf{g} = \left[\mathbf{g}^{(1)T} \ \mathbf{g}^{(2)T} \ \dots \ \left(\mathbf{g}^{(N_{\text{bs}})} \right)^T \right]^T$. The $PQ \times 1$ observation vector \mathbf{y} can now be re-written as,

$$\mathbf{y} = \mathbf{A} \Phi \mathbf{g} + \mathbf{n} = \mathbf{x} \Psi \mathbf{g} + \mathbf{n}, \quad (27)$$

with the sensing matrix $\Psi = \mathbf{A} \Phi$. Now, recovering the sparse vector \mathbf{g} from \mathbf{y} leads to recovering the non-zero entries in

the matrices $\{\mathbf{G}_i\}$, which solves the CD problem. We define support set, \mathcal{T}_i , for the vector \mathbf{g}_i as,

$$\mathcal{T}_i = \left\{ l \in \{1, \dots, N_t N_r\} \mid |\mathbf{g}_i^{(l)}|^2 > \delta \right\}.$$

Then, $\mathcal{T} = \bigcup_{i=1}^{N_{\text{bs}}} \mathcal{T}_i$ can be regarded as the support set of \mathbf{g} . The observation vector can be written as,

$$\mathbf{y} = \sum_{l_1 \in \mathcal{T}} [\Psi]_{:,l_1} \mathbf{g}_{l_1} x + \sum_{l_2 \notin \mathcal{T}} [\Psi]_{:,l_2} \mathbf{g}_{l_2} x + \mathbf{n}.$$

Now, detecting the presence of at least one BS is equivalent to verifying whether \mathbf{y} is generated by at least one column of Ψ indexed by \mathcal{T} . We declare that l^{th} entry in \mathbf{g} is non-zero whenever

$$\left| [\Psi]_{:,l}^* \mathbf{y} \right|^2 > \tau. \quad (28)$$

where τ is an appropriately chosen threshold. Denoting the detection metrics as $z_l = \left| [\Psi]_{:,l}^* \mathbf{y} \right|^2$, the false alarm probability and detection probability are given by

$$\mathbb{P}_F = \mathbb{P} \left(\bigcup_{l \notin \mathcal{T}} z_l > \tau \right) = \mathbb{P} \left(\max_{l \notin \mathcal{T}} z_l > \tau \right), \quad (29)$$

$$\mathbb{P}_D = \mathbb{P} \left(\bigcup_{l \in \mathcal{T}} z_l > \tau \right). \quad (30)$$

Mutual coherence parameter of the sensing matrix, defined as

$$\mu = \max_{l_1 \neq l_2} \frac{\left| [\Psi]_{:,l_1}^* [\Psi]_{:,l_2} \right|}{\left\| [\Psi]_{:,l_1} \right\|_2 \left\| [\Psi]_{:,l_2} \right\|_2}, \quad (31)$$

plays a significant role in the sparse signal recovery performance [18]. It is difficult to find the analytical expression for the probability of false alarm. On the other hand, detection probability is characterized below.

Theorem 2. *Under the idealized channel conditions in (3),(4), the probability of detection (\mathbb{P}_D) for the detector (28) using the observations (27) is given by,*

$$\begin{aligned} \mathbb{P}_D &= 1 - \prod_{k=1}^{|\mathcal{T}|} \left[1 - e^{-\frac{\tau}{\lambda_k}} \right] \\ &\geq 1 - \prod_{k=1}^{|\mathcal{T}|} \left[1 - \exp \left(-\frac{\tau}{\rho \sigma_{\min}^2 \bar{\mu}^2 + \sigma_n^2 \bar{\mu}} \right) \right], \end{aligned}$$

where λ_k 's are the eigen values of the matrix $\rho (\Psi_{\mathcal{T}}^* \Psi_{\mathcal{T}}) \mathbf{D} (\Psi_{\mathcal{T}}^* \Psi_{\mathcal{T}}) + \sigma_n^2 (\Psi_{\mathcal{T}}^* \Psi_{\mathcal{T}})$, \mathbf{D} is a diagonal matrix with the i^{th} diagonal element being the variance of \mathbf{g}_i with $i \in \mathcal{T}$, $\sigma_{\min}^2 = \min_k \{\mathbf{D}\}_{k,k}$, $\bar{\mu} = 1 - (|\mathcal{T}| - 1)\mu$, μ is the mutual coherence of Ψ .

Proof: Refer to Appendix B. ■

Smaller the value of μ , better is the recovery performance. First, we look at the mutual coherence value for the beam sweep and its variations discussed in the previous section. Next, we design two new training schemes which lead to smaller mutual coherence.

B. Beam Sweep and Variations:

For the conventional beam sweep, the resulting sensing matrix is given by $\Psi = \mathbf{1}_{N_{\text{bs}}}^T \otimes \mathbf{I}_{N_t N_r}$, which is a horizontal concatenation of identity matrices. The corresponding mutual coherence is 1, which is the worst case value. In the B-S technique, with all the BSs using the same beamforming vectors and pilot symbols, we can not differentiate between the signals between different BSs, and hence we get the worst case $\mu = 1$. This matches with our initial conclusion that B-S technique can not find the identity of the detected BS in the CD process. On the other hand, the columns of Ψ for different AoA-AoD pairs (different locations in \mathbf{G}_i) are orthogonal. Hence, conventional B-S will have the best performance in finding the AoA-AoD alignment between the detected BS and UE. We also note that the detector in (28) is identical to (12).

For the BC method, the resulting sensing matrix $\Psi = \mathbf{1}_{N_{\text{bs}}}^T \otimes \left[\left(\mathbf{I}_{\frac{N_t}{\beta_t}} \otimes \mathbf{1}_{\beta_t}^T \right) \otimes \left(\mathbf{I}_{\frac{N_r}{\beta_r}} \otimes \mathbf{1}_{\beta_r}^T \right) \right]$. Here also, $\mu = 1$ and hence distinction between different BSs is not possible. In addition, multiple DFT bins (of total size $\beta_r \times \beta_t$) get mapped to a single observation. Hence, AoA-AoD resolution within the grid of size $\beta_r \times \beta_t$ is not possible.

For the differential encoding based beam sweep, concatenating the two sets of observations from (10) and (23), the resulting sensing matrix is

$$\Psi = \frac{1}{\sqrt{2}} \begin{bmatrix} 1 & 1 & \dots & 1 \\ x_1 & x_2 & \dots & x_{N_{\text{bs}}} \end{bmatrix} \otimes \mathbf{I}_{N_t N_r}, \quad (32)$$

with $x_i = e^{j \frac{2\pi i}{(N_{\text{bs}}+1)}}$, $i = 1, \dots, N_{\text{bs}}$. The mutual coherence is $\mu = \sqrt{\frac{1}{2} \left[1 + \cos \left(\frac{2\pi}{N_{\text{bs}}+1} \right) \right]} < 1$. Since $\mu < 1$, this scheme can recover both the identity as well as AoA-AoD alignment of the detected BS. However, as N_{bs} increases, μ gets closer to 1, because the minimum distance of the $(N_{\text{bs}} + 1)$ -ary PSK constellation goes closer to 0.

C. Training Design using Mutually Unbiased Bases:

Mutually unbiased bases were originally developed in quantum information theory. A set of $d \times d$ matrices $\mathbf{B}_1, \mathbf{B}_2, \dots, \mathbf{B}_d$ are said to be mutually unbiased bases, if,

$$\mathbf{B}_l^* \mathbf{B}_l = \mathbf{I}_d, \forall l = 1, \dots, d, \text{ and} \\ \left| [\mathbf{B}_{i_1}]_{:,l}^* [\mathbf{B}_{i_2}]_{:,k} \right| = \frac{1}{\sqrt{d}}, \forall i_1 \neq i_2; l, k = 1, \dots, d.$$

In the above, $d = p^n$, where p is a prime number and n is a non-negative integer [17], [23].

We design training phase beamforming vectors using MUB matrices of sizes $\frac{N_t}{2^u} \times \frac{N_t}{2^u}$ and $N_r \times N_r$. Here, u is a non-negative integer, which is a design parameter controlling the training phase duration $M = \frac{N_t N_r}{2^u}$ and the total number of BS supported by our design $N_{\text{bs}} < \frac{N_t}{2^{2u}}$. Let $\{\mathbf{M}_q\}_{q=1}^{2^u N_{\text{bs}}}$ be a collection of $\frac{N_t}{2^u} \times \frac{N_t}{2^u}$ MUB matrices and \mathbf{M} be an $N_r \times N_r$ (unitary) MUB matrix. For each $i = 1, \dots, N_{\text{bs}}$, define matrices $\mathbf{M}^{(i)} = \left[\mathbf{M}_{(i-1)2^u+1} \mid \mathbf{M}_{(i-1)2^u+2} \mid \dots \mid \mathbf{M}_{i2^u} \right]$. With $Q = \frac{N_t}{2^u}, P = N_r$, we propose the following design for the

training beamforming vectors,

$$\mathbf{w}_r^{(p)} = \mathbf{F}_{N_r} \left([\mathbf{M}]_{p,:} \right)^*, p = 1, \dots, P, \quad (33)$$

$$\mathbf{w}_{t_i}^{(q)} = \mathbf{F}_{N_t} \left([\mathbf{M}^{(i)}]_{q,:} \right)^T, q = 1, \dots, Q, \quad (34)$$

and we refer this MUB based beamforming as MUBB technique. We take measurements for *all* the combinations of transmit/receive beamforming pairs, resulting in a total number of observations $M = \frac{N_t N_r}{2^u}$. Note that $\|\mathbf{w}_r^{(p)}\|_2^2 = 1, \forall p$ and $\|\mathbf{w}_{t_i}^{(q)}\|_2^2 = 2^u, \forall q, i$. This ensures that the total power (squared norm) of the transmit beamforming vectors at each BS for the entire training phase is $N_t N_r$. Setting the resulting sensing matrix $\Psi = [\Psi_1 \mid \Psi_2 \mid \dots \mid \Psi_{N_{\text{bs}}}]$, where Ψ_i are $M \times N_t N_r$ matrices defined as,

$$\Psi_i = \mathbf{M}^{(i)} \otimes \mathbf{M} = \left[\mathbf{M}_{(i-1)2^u+1} \otimes \mathbf{M} \mid \dots \mid \mathbf{M}_{i2^u} \otimes \mathbf{M} \right],$$

the overall Ψ matrix turns out to be,

$$\Psi = \left[\mathbf{M}_1 \otimes \mathbf{M} \mid \mathbf{M}_2 \otimes \mathbf{M} \mid \dots \mid \mathbf{M}_{2^u N_{\text{bs}}} \otimes \mathbf{M} \right]. \quad (35)$$

Theorem 3. *The sensing matrix Ψ constructed according to equation (35) has the following properties:*

- 1) For each $q = 1, 2, \dots, 2^u N_{\text{bs}}$, $\mathbf{M}_q \otimes \mathbf{M}$ is a unitary matrix.
- 2) The mutual coherence of the Ψ matrix is equal to $\sqrt{\frac{2^u}{N_t}}$.

Proof: Refer to Appendix C. ■

We note that the mutual coherence of MUB design is inversely proportional to $\sqrt{N_t}$. For large antenna arrays at the BS, we get small values for μ as long as $N_{\text{bs}} < \frac{N_t}{2^{2u}}$. On the other hand, μ of differential encoding sensing matrix (32) does not depend on N_t and it always increases with N_{bs} .

D. Random Beamforming:

In the compressive sensing theory [16], [24], it has been established that any randomly generated matrix will have low mutual coherence with high probability. In the random beamforming (RBF), we generate the beamforming vectors randomly, using i.i.d. Rademacher entries. Details are given below. In the RBF scheme, both transmitter and receiver change their beamforming vectors at every time instant. The set of M observations are obtained as

$$y_m = \mathbf{w}_r^{(m)*} \sum_{i=1}^{N_{\text{bs}}} \mathbf{H}_i \mathbf{w}_{t_i}^{(m)} x + n_m, m = 1, \dots, M. \quad (36)$$

Setting $M = \frac{N_t N_r}{2^u}$, we describe the design the beamforming vectors $\{\mathbf{w}_r^{(m)}\}$ and $\{\mathbf{w}_{t_i}^{(m)}\}_{i=1}^{N_{\text{bs}}}, \forall m$, using Rademacher entries.

- Set $\mathbf{w}_{t_i}^{(m)} = \mathbf{F}_{N_t} \mathbf{v}_i^{(m)}$, where for each $i = 1, \dots, N_{\text{bs}}$ and $m = 1, \dots, M$, elements of the vector $\mathbf{v}_i^{(m)}$ are chosen from $\left\{ \pm \sqrt{\frac{2^u}{N_t}} \right\}$ uniformly at random. It can be verified that the total power (squared norm) of the transmit beamforming vectors is $N_t N_r$, same as that of conventional beam sweep.
- Similarly, choose $\mathbf{w}_r^{(m)}$ as $\mathbf{F}_{N_r} \mathbf{u}^{(m)}$, where for each $m = 1, \dots, M$, entries in $\mathbf{u}^{(m)}$ are uniformly chosen from the

set $\left\{ \pm \frac{1}{\sqrt{N_r}} \right\}$. We note that the norm of $\mathbf{w}_r^{(m)}$, $\forall m$ is equal to 1.

It can be verified that the entries of resulting Ψ matrix are of the form $\pm \sqrt{\frac{2^u}{N_t N_r}}$. Mutual coherence of this matrix is characterized in [22]. Such design of training beamforming vectors using random entities are commonly used in mm wave channel estimation algorithms [15], [22], [25].

E. Extensions to Multiple RF Chains:

In our original system model (6), each BS and the UE employed one transmit and one receive beamforming vector respectively, for every observation instant. With a hybrid beamforming architecture [2], [15], using digital baseband processors, multiple RF chains can be supported with ULA, for nominal costs. With multiple RF chains at the receiver, by using different receive beamforming vectors, we can get multiple received observations at a single time instant. Suppose $\mathbf{w}_r^{(p,s)}$ is the receive beamforming vector used at the UE for the s^{th} RF chain, then the measurement obtained is given by,

$$y_{p,q}^{(s)} = \mathbf{w}_r^{(p,s)*} \left(\sum_{i=1}^{N_{\text{bs}}} \mathbf{H}_i \mathbf{w}_{t_i}^{(q)} x_{p,q}^{(i)} \right) + \underbrace{\mathbf{w}_r^{(p,s)H} \mathbf{n}_{p,q}}_{n_{p,q}^{(s)}}, \quad (37)$$

where $p \in \{1, 2, \dots, P\}$, $q \in \{1, 2, \dots, Q\}$ and $s \in \{1, 2, \dots, N_{\text{rf}}\}$, with N_{rf} being the number of RF chains at the UE and $\mathbf{n}_{p,q}$ is the AWGN noise vector at the time instant indexed by (p, q) . By suitably choosing the beamforming vectors of the RF chains, the overall duration of the training phase to get M observations can be reduced to $\frac{M}{N_{\text{rf}}}$. For beam sweep and its variations, and MUB beamforming, the receive beamforming vectors at different RF chains $\{\mathbf{w}_r^{(p,s)}, s = 1, \dots, N_{\text{rf}}\}$ at a particular instant (p, q) can be chosen as orthonormal vectors. Hence, the noise samples $n_{p,q}^{(s)}$ are i.i.d. Gaussian. While the training phase gets reduced with multiple RF chains, the performance of beam sweep and its variations, and MUBB do not get affected. On the other hand, for RBF, the randomly generated receive beamforming vectors are not orthogonal and hence $n_{p,q}^{(s)}$ is correlated across s . In addition, the mutual coherence parameter of the sensing matrix in RBF increases with the number of RF chains, as the entries in Ψ gets more correlated. Due to these issues, the performance of RBF degrades with increase in N_{rf} . This fact is validated via simulation results in the following section.

V. SIMULATION RESULTS

In this section, we present our simulation results comparing the performance of various cell discovery algorithms in terms of probability of successful detection \mathbb{P}_D with a constraint on the probability of false alarm \mathbb{P}_F .

A. Verifying the derived \mathbb{P}_D expressions using simulations:

We first validate the expressions obtained for the detection probability \mathbb{P}_D for all the methods, using simulations. The results are plotted in Figure 1. Here, we fix $N_t = 64$, $N_r = 8$. We vary $N_{\text{bs}} = 2, 4$ for the B-S method, while we fix it to

be 4 for MUBB and RBF methods. We considered multi-path scenario with $K_1 = 3, K_2 = 4, K_3 = K_4 = 2$ whenever $N_{\text{bs}} = 4$, for all the techniques where we generate the channel gains as $\mathcal{CN}(0, \sigma_{k_i}^2)$, with $\sigma_{k_i}^2 = \frac{N_t N_r}{K_i} \alpha$ and $\alpha \in (0, 1)$, $\forall i, k$. When $N_{\text{bs}} = 2$, we set $K_1 = 3, K_2 = 4$. We also considered single path case for the MUBB and RBF methods. We observe that under *idealized channel assumptions*, the derived expressions exactly match with the simulation curves for the proposed training schemes.

B. Network Setup and Non-ideal Channels:

In order to do detailed simulation studies, we consider the network set-up as shown in Figure 2. We assume a 4×4 square grid with each grid having length R meters. We deploy one BS in each grid at random location, and place a UE in one of the grids chosen uniformly at random (indicated by a green dot in Figure 2). Hence, we get $N_{\text{bs}} = 16$. In a practical environment, signals from many of the BSs will not reach the UE due to severe blockage effects in mm wave systems. Hence, we assume that the environment has only four active BSs, i.e., signals from only four BSs reach the given UE. These active BSs are picked randomly from the total 16 (indicated by red dots in the same figure) and the remaining inactive BSs (which are assumed to make zero channel with the UE) are indicated by the blue dots. We assume direct LOS link to exist between (randomly chosen) two of the active BSs and the UE. The other two active BSs have NLOS link with the UE.

The channel between each BS and UE is generated using NYUSIM simulator [20], [21] which is an experimentally driven spatial channel simulator for wideband mmwave communication systems. We assume the following parameters: $N_t = 256$, $N_r = 4$, $N_{\text{rf}} = 4$ and the operating carrier frequency is 28 GHz. The additive noise is modeled as thermal noise with noise variance given by kTB , where $T = 293$ kelvin is the operating temperature, $B = 800$ MHz is the system bandwidth and $k = 1.38 \times 10^{-23}$ J/K is the Boltzmann's constant. All other parameters in the NYUSIM graphical user interface are set to their default values.

For the purpose of simulations, we implement the BC method with $\beta_t = 2, \beta_r = 1$, leading to a total of $M = \frac{N_t N_r}{2}$ measurements. We consider differential encoding with beam sweep (DBS) which uses $2N_t N_r$ observations. We also consider differential encoding with beam combining (DBC) with two sets of parameters ($\beta_t = 2, \beta_r = 1$) and ($\beta_t = 4, \beta_r = 1$). The performance of all the training schemes are studied in terms of \mathbb{P}_D versus cell length R by averaging over 2500 realizations of the above described network set-up. We fix non-zero threshold δ in equation (11) as $\delta = \frac{1}{2} \left(\max_{1 \leq l_1 \leq N_r; 1 \leq l_2 \leq N_t} |[\mathbf{G}_i]_{l_1, l_2}|^2 \right)$, and the threshold τ for the detectors are chosen as,

$$\tau = \begin{cases} \kappa \left(\max_{1 \leq p \leq P; 1 \leq q \leq Q} |y_{p,q}|^2 \right), & \text{for methods in Section III,} \\ \kappa \|\Psi^H \mathbf{y}\|_{\infty}^2, & \text{for schemes in Section IV} \end{cases}$$

Here, κ is chosen s.t. the probability of false alarm (\mathbb{P}_F) is 0.1. Note that the value of κ will vary across different techniques.

N_{bs}	B-S, BC, DBC ($\forall M, N_{rf}$)	DBS ($M = 2048, \forall N_{rf}$)		MUBB ($\forall N_{rf}$)	RBF		
					$N_{rf} = 1$	$N_{rf} = 2$	$N_{rf} = 4$
16	1	0.9830	$M = 1024 \rightarrow$	0.0625	0.1641	0.2148	0.2969
			$M = 512 \rightarrow$	0.0884	0.2305	0.3047	0.4219
			$M = 256 \rightarrow$	0.125	0.3281	0.4219	0.5938
32	1	0.9955	$M = 1024 \rightarrow$	0.0625	0.1719	0.2305	0.3203
			$M = 512 \rightarrow$	0.0884	0.2422	0.3203	0.4531

TABLE I: Mutual coherence (μ) values of the Ψ matrix in different schemes with $N_t = 256$ and $N_r = 4$.

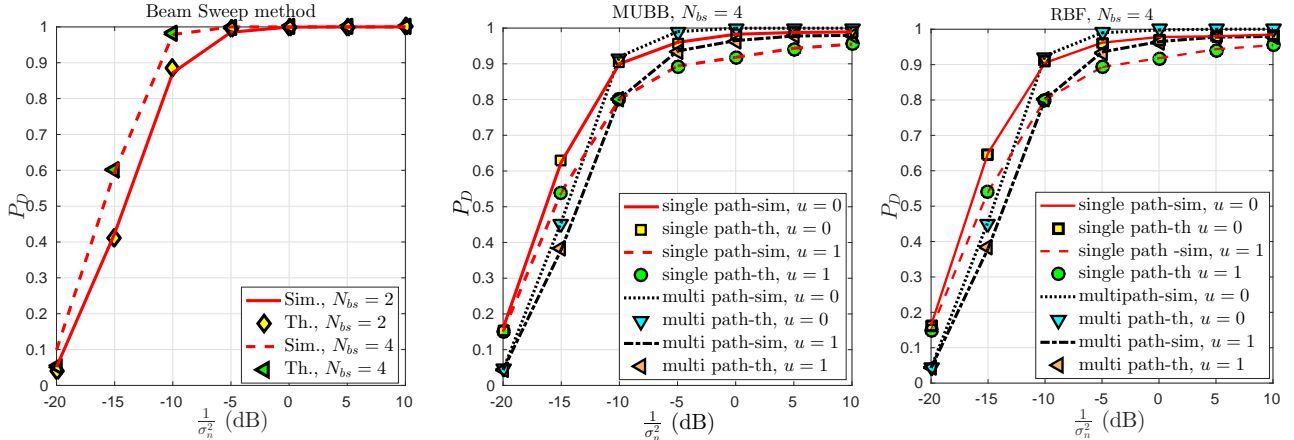


Fig. 1: Verifying the expressions derived for \mathbb{P}_D , with $N_t = 64, N_r = 8, \mathbb{P}_F = 0.01$. For multi-path case $K_1 = 3, K_2 = 4, K_3 = K_4 = 2$ when $N_{bs} = 4$, and $K_1 = 3, K_2 = 4$ when $N_{bs} = 2$.

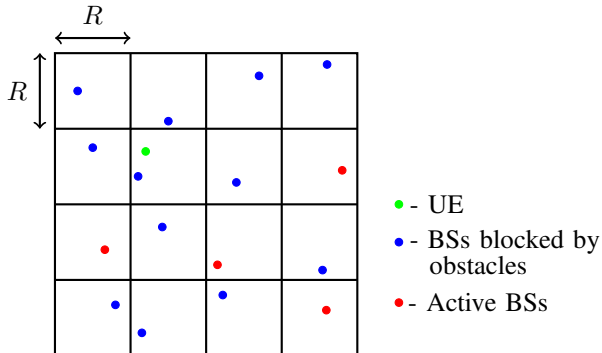


Fig. 2: Network set-up considered for one realization/iteration during simulations.

The mutual coherence (μ) values of the Ψ matrix for different training schemes are listed in TABLE I. Recall that the structure of Ψ is deterministic for all the schemes except for the RBF method. So, for simulating the RBF method, we choose the best Ψ matrix (the one with the smallest μ value, which is specified in TABLE I) among 2000 random realizations. Note that the μ of the Ψ matrix constructed using MUBs is the smallest for any given M . Hence, MUBB is expected to exhibit better performance compared to other methods.

C. Comparison of different training schemes:

We plot the \mathbb{P}_D performance of all the proposed pilot training methods w.r.t. R in Figure 3(a). We fix $N_{bs} = 16$. We observe that the performance of all the schemes decreases

with R , mainly due to decrease in the value of SNR at the UE. We observe that the B-S scheme and the MUBB method with $u = 0$ outperform all the other techniques. Even with reduced number of measurements M (setting $u = 1, 2$), the MUBB method provides considerably good detection performance in terms of \mathbb{P}_D . In fact, it is comparable with the B-S technique for $R \leq 550$ meters. This is mainly because of the low value of μ achieved in MUBB method. We also observe that for MUBB method (with various values of M) is better than the corresponding DBC and RBF techniques, which use the same number of measurements. The performance of the differential encoding schemes highly depends on the SNR and N_{bs} . Since SNR decays with R , \mathbb{P}_D of DBS and DBC schemes decrease as a function of R .

D. Successful detection of the strongest BS in the network:

We also study the efficiency of the proposed pilot training strategies in detecting the strongest BS in the network. The BS with the largest magnitude entry in the \mathbf{G}_i matrix is termed as the *strongest BS* and the corresponding path with the largest gain is termed as the *strongest path*. We now define the success probability (\mathbb{P}_D) of a training scheme as the probability of detecting the strongest base station and the AoA-AoD alignment of the strongest path. Strongest path of the strongest BS is identified by the largest value of the metric in (28). From Figure 3(c), we observe that the MUBB method with $M = 1024$ outperforms all the other schemes. In addition, MUBB method implemented with reduced training overhead $M = 512$ performs better than DBC and RBF techniques with larger training overhead $M = 1024$.

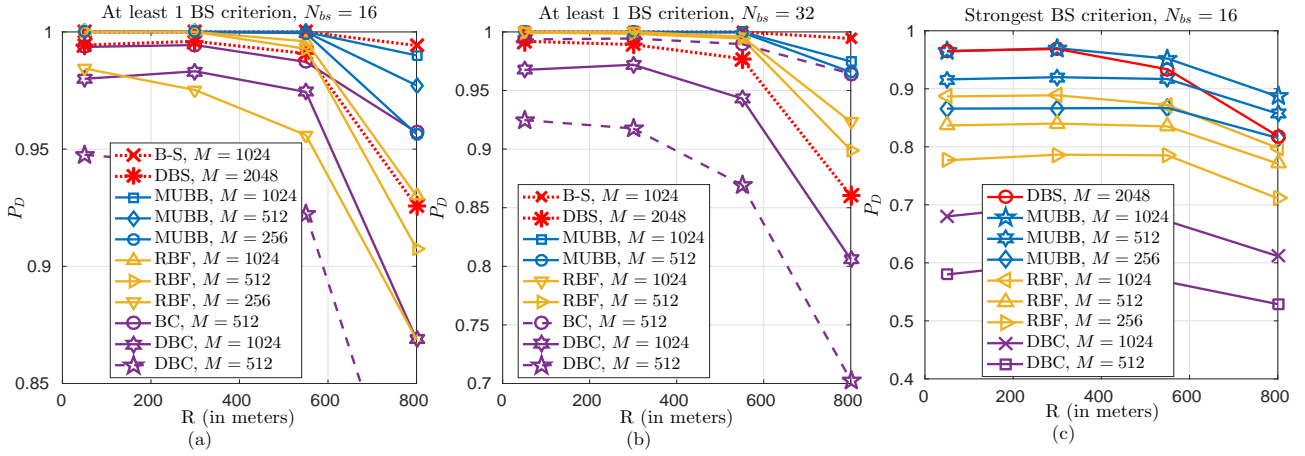


Fig. 3: Comparison of all the pilot training methods in terms \mathbb{P}_D for, (a) detecting at least one accessible BS assuming $N_{bs} = 16$, (b) detecting at least one accessible BS assuming $N_{bs} = 32$ and (c) detecting the strongest active BS for $N_{bs} = 16$, w.r.t. R with $N_t = 256$, $N_r = 4$, $\mathbb{P}_F = 0.1$, $N_{rf} = 4$.

E. Impact of multiple RF chains:

Presence of multiple RF chains do not affect the behavior of the \mathbb{P}_D curves for all the methods, except RBF. This is, once again, due to the increase in the mutual coherence of the RBF sensing matrix Ψ with the number of RF chains. This is verified in Figure 4, where we plotted the detection probability of the RBF and MUBB techniques for the two criterions: (i) successfully detecting at least one accessible BS, and (ii) successfully detecting the strongest BS. With increase in the value of N_{rf} , the detection probability of the RBF method decreases.

F. Beamforming gains for different training schemes:

Based on the strongest detected BS and the corresponding AoA-AoD pair, we can choose the optimal beam directions to be used by BS and UE during the subsequent data transmission phase. In this section, we study the *beamforming gain* achieved by the various training schemes, using the optimal beamforming vectors. Let (p_0, q_0) corresponds to an AoA-AoD pair of the strongest path corresponding to the strongest detected BS i_0 , based on the largest value of the metric in (28). With the optimal beamforming vectors $\mathbf{w}_t = [\mathbf{F}_{N_t}]_{:,q_0}$ and $\mathbf{w}_r = [\mathbf{F}_{N_r}]_{:,p_0}$, the corresponding *beamforming gain* is given by $|\mathbf{w}_r^H \mathbf{H}_{i_0} \mathbf{w}_t|$. For the DBC technique, since combined beams are used in the search process, the resolution of the detected AoA-AoD pair is limited to a submatrix (in the 2D DFT grid) of size $\beta_r \times \beta_t$. In this case, the optimal beamforming vectors are chosen as the weighted sum of the columns of the corresponding DFT bins, as in (18) and (19). However, the scaling factor in (19) need to be changed to make the beamforming vector to be of unit norm.

Figure 5 illustrates the simulation result in terms of the cumulative distribution function (CDF) of the *beamforming gain* for different values of R and M . As expected, when R increases the achievable beamforming gain decreases for all methods, and hence the CDF value attains 1 at lower values of the gain. The performance of the MUBB and RBF methods

are exactly the same as shown in the figure. Since the DBC method uses wider beams during training, the resolution of the estimated AoA-AoD angles will be less. Hence for a given R , the *beamforming gain* for the DBC algorithm will be lower compared to the other techniques. Next, while the CDF plots for the MUBB and RBF techniques remain unaffected when M is reduced from 1024 to 512, the reduction in M results in even wider transmit and receive training beams in case of the DBC technique. As a result, its *beamforming gain* value reduces further. Since the B-S and BC techniques discussed in this paper cannot retrieve exact information about active BSs' identities, we do not compute the *beamforming gain* for these methods.

VI. CONCLUSION

In this article, we addressed the cell discovery problem in millimeter wave communication systems. We considered several existing and new pilot training schemes. We presented the physical layer implementations of all these schemes, by explicitly specifying the transmit/receiver beamforming vectors in the training phase and developed receiver algorithms to detect at least one potential BS in the network. Using this framework, we obtained analytical characterization of the detection probability of all these schemes and also obtained simulation results using channels from NYUSIM. Our results showed that our proposed MUB based beamforming method is superior to all the other techniques in terms of both detection probability and training overhead. Our future work will be based on incorporating timing and frequency offset effects in the system model, and addressing the mm wave cell discovery problem using advanced sparse signal recovery algorithms.

APPENDIX

A. Proof of Theorem 1:

Under the *idealized channel assumption*, 2D Fourier domain channel matrix \mathbf{G}_i will have exactly K_i non-zero bins. The variance of the entry in a given bin will be equal to the variance

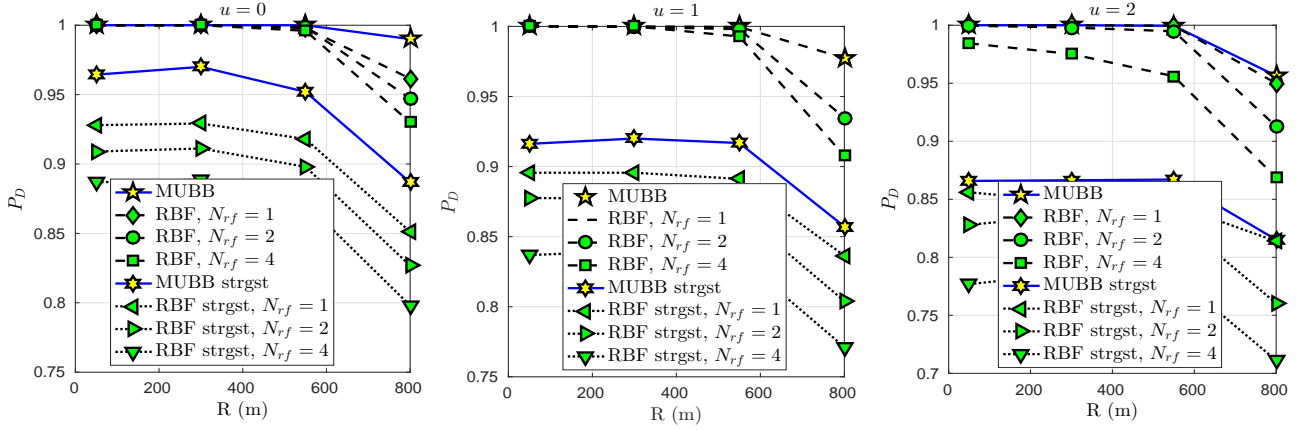


Fig. 4: Studying the impact of multiple RF chains in the \mathbb{P}_D performance of RBF training scheme.

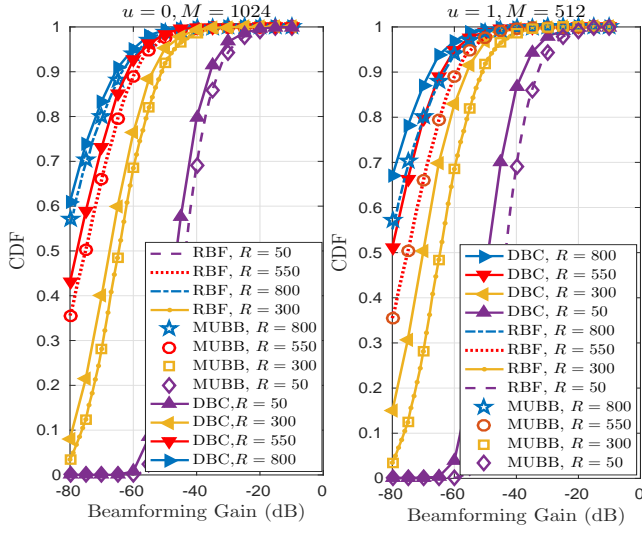


Fig. 5: CDF of *beamforming gain* for different training schemes w.r.t R and M , with $N_t = 256$, $N_r = 4$, $N_{bs} = 16$.

$\sigma_{k_i}^2$ of the path whose spatial frequency pair match with the bin frequency pair.

- **Non-overlap case:**

Since $\bigcap_{i=1}^{N_{bs}} \mathcal{S}_i = \emptyset$, the observations $y_{p,q}$, $\forall p, q$ defined in equation (10) are given by,

$$y_{p,q} = \begin{cases} x_{p,q}^{(i)} [\mathbf{G}_i]_{p,q} + n_{p,q}, & \text{if } (p, q) \in \mathcal{S}, \\ n_{p,q}, & \text{if } (p, q) \notin \mathcal{S}, \end{cases}$$

for some $i \in \{1, 2, \dots, N_{bs}\}$. In fact, the value of i depends on the tuple (p, q) . Thus, \mathbb{P}_F can be derived as,

$$\begin{aligned} \mathbb{P}_F &= \mathbb{P}\left(\max_{(p,q) \notin \mathcal{S}} |y_{p,q}|^2 > \tau\right) \\ &= 1 - \mathbb{P}\left(\max_{(p,q) \notin \mathcal{S}} |y_{p,q}|^2 \leq \tau\right) \\ &= 1 - \mathbb{P}\left(\max_{(p,q) \notin \mathcal{S}} |n_{p,q}|^2 \leq \tau\right), \end{aligned}$$

Since $n_{p,q}$ are all i.i.d. $\mathcal{CN}(0, \sigma_n^2)$, we get,

$$\begin{aligned} \mathbb{P}_F &= 1 - \prod_{(p,q) \notin \mathcal{S}} \mathbb{P}(|n_{p,q}|^2 \leq \tau) \\ &= 1 - \left(1 - e^{-\frac{\tau}{\sigma_n^2}}\right)^{N_t N_r - |\mathcal{S}|}. \end{aligned}$$

For any $(p, q) \in \mathcal{S}$, we have $y_{p,q} \sim \mathcal{CN}(0, \rho\sigma_{k_i}^2 + \sigma_n^2)$ for some k and i . In addition, these observations are independent. As the result, the detection probability \mathbb{P}_D is given by,

$$\begin{aligned} \mathbb{P}_D &= \mathbb{P}\left(\bigcup_{(p,q) \in \mathcal{S}} |y_{p,q}|^2 > \tau\right) = 1 - \mathbb{P}\left(\bigcap_{(p,q) \in \mathcal{S}} |y_{p,q}|^2 \leq \tau\right) \\ &= 1 - \prod_{(p,q) \in \mathcal{S}} \mathbb{P}(|y_{p,q}|^2 \leq \tau) \\ &= 1 - \prod_{i \in \{1, \dots, N_{bs}\}, k \in \{1, \dots, K_i\}} \left(1 - e^{-\frac{\tau}{\rho\sigma_{k_i}^2 + \sigma_n^2}}\right). \end{aligned}$$

- **Overlap case:**

The expression for the probability of false alarm \mathbb{P}_F can be derived in the same way as in **Non-overlap case**. We now derive a lower bound on the probability of detection.

$$\begin{aligned} \mathbb{P}_D &= \mathbb{P}\left(\bigcup_{(p,q) \in \mathcal{S}_{\text{actv}}} |y_{p,q}|^2 > \tau\right) \\ &\geq \mathbb{P}\left(|y_{\tilde{p}, \tilde{q}}|^2 > \tau\right), \text{ for every } (\tilde{p}, \tilde{q}) \in \mathcal{S}_{\text{actv}} \\ &= e^{-\frac{\tau}{\kappa_{\tilde{p}, \tilde{q}}^2}}, \text{ for every } (\tilde{p}, \tilde{q}) \in \mathcal{S}_{\text{actv}}, \end{aligned}$$

where $\kappa_{p,q}^2$ is the variance of $y_{p,q}$, $\forall (p, q) \in \mathcal{S}_{\text{actv}}$. Thus, we get,

$$\begin{aligned} \mathbb{P}_D &\geq \max_{(p,q) \in \mathcal{S}_{\text{actv}}} e^{-\frac{\tau}{\kappa_{p,q}^2}} = \exp\left(-\left[\min_{(p,q) \in \mathcal{S}_{\text{actv}}} \frac{\tau}{\kappa_{p,q}^2}\right]\right) \\ &= \exp\left(-\frac{\tau}{\max_{(p,q) \in \mathcal{S}_{\text{actv}}} \kappa_{p,q}^2}\right). \end{aligned} \quad (38)$$

As mentioned before, each of the active symbols is generated by at least one non-zero entry of the sparse matrices $\{\mathbf{G}_i\}_{i=1}^{N_{bs}}$. Assuming, $x_{p,q}^{(i)} = x$, $\forall p, q, i$, we

have,

$$\max_{(p,q) \in \mathcal{S}_{\text{actv}}} \kappa_{p,q}^2 \geq \rho \max_{i=\{1,\dots,N_{\text{bs}}\}, k=\{1,\dots,K_i\}} \sigma_{k_i}^2 + \sigma_n^2,$$

leading to the \mathbb{P}_D bound given in (17).

B. Proof of Theorem 2:

Probability of detection can be written as,

$$\begin{aligned} \mathbb{P}_D &= \mathbb{P}\left(\bigcup_{l \in \mathcal{T}} z_l > \tau\right) = 1 - \mathbb{P}\left(\bigcap_{l \in \mathcal{T}} z_l \leq \tau\right) \\ &= 1 - \mathbb{P}\left(\bigcap_{l \in \mathcal{T}} |[\tilde{\Psi}]_{:,l}^* \mathbf{y}|^2 \leq \tau\right). \end{aligned}$$

Let $\mathbf{z} = \Psi_{\mathcal{T}}^* \mathbf{y}$. One can verify that $\mathbf{z} \sim \mathcal{CN}(\mathbf{0}, \mathbf{C})$, where $\mathbf{C} = \rho(\Psi_{\mathcal{T}}^* \Psi_{\mathcal{T}}) \mathbf{D}(\Psi_{\mathcal{T}}^* \Psi_{\mathcal{T}}) + \sigma_n^2 (\Psi_{\mathcal{T}}^* \Psi_{\mathcal{T}})$ which is defined in the theorem. In general, \mathbf{C} is not a diagonal matrix. Since \mathbf{C} is a hermitian matrix, its eigen value decomposition can be written as $\mathbf{C} = \tilde{\mathbf{U}} \tilde{\mathbf{D}} \tilde{\mathbf{U}}^*$, where $\tilde{\mathbf{U}}$ is a unitary matrix containing eigenvectors of \mathbf{C} and $\tilde{\mathbf{D}}$ a diagonal matrix with eigenvalues of \mathbf{C} as its diagonal entries. Define $\tilde{\mathbf{z}} = \tilde{\mathbf{U}}^* \mathbf{z}$. Clearly, $\mathbb{E}[\tilde{\mathbf{z}}] = \mathbf{0}$. And, $\mathbb{E}[\tilde{\mathbf{z}} \tilde{\mathbf{z}}^*] = \tilde{\mathbf{U}}^* \mathbb{E}[\mathbf{z} \mathbf{z}^*] \tilde{\mathbf{U}} = \tilde{\mathbf{U}}^* \mathbf{C} \tilde{\mathbf{U}} = \tilde{\mathbf{D}} \Rightarrow \tilde{\mathbf{z}} \sim \mathcal{CN}(\mathbf{0}, \tilde{\mathbf{D}})$, i.e., entries in $\tilde{\mathbf{z}}$ are independent.

Consider the event $\bigcap_{k=1}^{|\mathcal{T}|} |\tilde{\mathbf{z}}_k|^2 \leq \tau$. Now, magnitude square value of the k^{th} element of $\tilde{\mathbf{z}}$ is bounded as,

$$|\tilde{\mathbf{z}}_k|^2 = |[\tilde{\mathbf{U}}]_{:,k}^* \mathbf{z}|^2 \leq \sum_{i=1}^{|\mathcal{T}|} |[\tilde{\mathbf{U}}]_{i,k}|^2 |\mathbf{z}_i|^2 \leq \tau \|[\tilde{\mathbf{U}}]_{:,k}\|_2^2 = \tau.$$

Note that the above holds true for all elements of $\tilde{\mathbf{z}}$. Thus, we conclude that the event $\left\{\bigcap_{k=1}^{|\mathcal{T}|} |\tilde{\mathbf{z}}_k|^2 \leq \tau\right\}$ leads to the event

$\left\{\bigcap_{k=1}^{|\mathcal{T}|} |\tilde{\mathbf{z}}_k|^2 \leq \tau\right\}$. Since matrix $\tilde{\mathbf{U}}$ being unitary, we also have,

$\mathbf{z} = \tilde{\mathbf{U}} \tilde{\mathbf{z}}$, and as a result, the event $\left\{\bigcap_{k=1}^{|\mathcal{T}|} |\tilde{\mathbf{z}}_k|^2 \leq \tau\right\}$ will give

rise to $\left\{\bigcap_{k=1}^{|\mathcal{T}|} |\mathbf{z}_k|^2 \leq \tau\right\}$. Hence, $\mathbb{P}\left(\bigcap_{l \in \mathcal{T}} |[\Psi]_{:,l}^* \mathbf{y}|^2 \leq \tau\right) =$

$\mathbb{P}\left(\bigcap_{k=1}^{|\mathcal{T}|} |\mathbf{z}_k|^2 \leq \tau\right) = \mathbb{P}\left(\bigcap_{k=1}^{|\mathcal{T}|} |\tilde{\mathbf{z}}_k|^2 \leq \tau\right)$. It can be verified

that $\left\{|\tilde{\mathbf{z}}_k|^2\right\}_{k=1}^{|\mathcal{T}|}$ are independent exponential random variables with parameters $\frac{1}{[\tilde{\mathbf{D}}]_{k,k}}$ respectively. So, we finally get,

$$\mathbb{P}_D = 1 - \mathbb{P}\left(\bigcap_{k=1}^{|\mathcal{T}|} |\tilde{\mathbf{z}}_k|^2 \leq \tau\right) = 1 - \prod_{k=1}^{|\mathcal{T}|} \left[1 - e^{-\frac{\tau}{[\tilde{\mathbf{D}}]_{k,k}}}\right].$$

The λ_k 's stated in the theorem are the $[\tilde{\mathbf{D}}]_{k,k}$'s mentioned above. To derive the lower bound, we consider the matrix $\mathbf{C}_{\min} = \rho d_{\min} \mathbf{T}^2 + \sigma_n^2 \mathbf{T}$, where $d_{\min} = \min_{1 \leq k \leq |\mathcal{T}|} [\tilde{\mathbf{D}}]_{k,k}$ and $\mathbf{T} = \Psi_{\mathcal{T}}^* \Psi_{\mathcal{T}}$. Then, the following facts can be verified. The minimum eigen value of \mathbf{C} , i.e., $\min_{1 \leq k \leq |\mathcal{T}|} [\tilde{\mathbf{D}}]_{k,k}$, is greater than the minimum eigen value of \mathbf{C}_{\min} . If λ is an eigen value of \mathbf{T} with some eigen vector, then \mathbf{C}_{\min} will have the same eigen vector with corresponding eigen value being $\rho d_{\min} \lambda^2 + \sigma_n^2 \lambda$. Lastly, every eigen value of \mathbf{T} can be lower bounded by $1 -$

$(|\mathcal{T}| - 1)\mu$ using Gershgorin's circle theorem [26], where μ is the mutual coherence of Ψ . All these implies,

$$\begin{aligned} [\tilde{\mathbf{D}}]_{k,k} &\geq \min_{1 \leq l \leq |\mathcal{T}|} [\tilde{\mathbf{D}}]_{l,l} \geq \text{min. eigen value of } \mathbf{C}_{\min} \\ &\geq \rho d_{\min} \left[1 - (|\mathcal{T}| - 1)\mu\right]^2 + \sigma_n^2 \left[1 - (|\mathcal{T}| - 1)\mu\right]. \end{aligned}$$

Lower bounding $[\tilde{\mathbf{D}}]_{k,k}$, which are present in the \mathbb{P}_D expression, will in turn, gives the lower bound for \mathbb{P}_D as stated in the theorem. Hence, proved.

C. Proof of Theorem 3:

Here, we prove the properties of Ψ matrix constructed using MUBs.

1) We have,

$$\begin{aligned} (\mathbf{M}_q \otimes \mathbf{M})^* (\mathbf{M}_q \otimes \mathbf{M}) &= (\mathbf{M}_q^* \mathbf{M}_q) \otimes (\mathbf{M}^* \mathbf{M}) \\ &= \mathbf{I}_{\frac{N_t}{2^u}} \otimes \mathbf{I}_{N_r} = \mathbf{I}_M. \end{aligned}$$

In the above, third equality is obtained using the fact that matrices \mathbf{M}_q and \mathbf{M} are unitary.

2) For any $q, \bar{q} \in \{1, \dots, 2^u N_{\text{bs}}\}$ and $q \neq \bar{q}$, we have,

$$\begin{aligned} (\mathbf{M}_q \otimes \mathbf{M})^* (\mathbf{M}_{\bar{q}} \otimes \mathbf{M}) &= (\mathbf{M}_q^* \mathbf{M}_{\bar{q}}) \otimes (\mathbf{M}^* \mathbf{M}) \\ &= \sqrt{\frac{2^u}{N_t}} \mathbf{Q} \otimes \mathbf{I}_{N_r}, \end{aligned}$$

where \mathbf{Q} is some matrix with absolute value of all its entries being 1. It can, therefore, be said that magnitude of inner product of two different columns of Ψ matrix is equal to either zero or $\sqrt{\frac{2^u}{N_t}}$. Thus, mutual coherence of Ψ equals $\sqrt{\frac{2^u}{N_t}}$.

REFERENCES

- [1] M. Xiao, S. Mumtaz, Y. Huang, L. Dai, Y. Li, M. Matthaiou, G. K. Karagiannidis, E. Bjrnson, K. Yang, C. I, and A. Ghosh, "Millimeter Wave Communications for Future Mobile Networks," *IEEE J. Sel. Areas Commun.*, vol. 35, no. 9, pp. 1909–1935, 2017.
- [2] O. E. Ayach, S. Rajagopal, S. Abu-Surra, Z. Pi, and R. W. Heath, "Spatially Sparse Precoding in Millimeter Wave MIMO Systems," *IEEE Trans. Wireless Commun.*, vol. 13, no. 3, pp. 1499–1513, 2014.
- [3] J. Zhang, A. Beletchi, Y. Yi, and H. Zhuang, "Capacity performance of millimeter wave heterogeneous networks at 28GHz/73GHz," in *Proc. GLOBECOM*, pp. 405–409, Dec. 2014.
- [4] C. N. Barati, S. A. Hosseini, M. Mezzavilla, T. Korakis, S. S. Panwar, S. Rangan, and M. Zorzi, "Initial Access in Millimeter Wave Cellular Systems," *IEEE Trans. Wireless Commun.*, Dec. 2016.
- [5] S. Hur, T. Kim, D. J. Love, J. V. Krogmeier, T. A. Thomas, and A. Ghosh, "Millimeter Wave Beamforming for Wireless Backhaul and Access in Small Cell Networks," *IEEE Trans. Commun.*, 2013.
- [6] C. N. Barati, S. A. Hosseini, S. Rangan, P. Liu, T. Korakis, S. S. Panwar, and T. S. Rappaport, "Directional Cell Discovery in Millimeter Wave Cellular Networks," *IEEE Trans. Wireless Commun.*, Dec. 2015.
- [7] V. Raghavan, J. Cezanne, S. Subramanian, A. Sampath, and O. Koymen, "Beamforming Tradeoffs for Initial UE Discovery in Millimeter-Wave MIMO Systems," *IEEE J. Sel. Topics Signal Process.*, 2016.
- [8] I. Filippini, V. Sciancalepore, F. Devoti, and A. Capone, "Fast Cell Discovery in mm-Wave 5G Networks with Context Information," *IEEE Trans. Mobile Comput.*, vol. 17, no. 7, pp. 1538–1552, 2018.
- [9] F. Devoti, I. Filippini, and A. Capone, "Facing the Millimeter-Wave Cell Discovery Challenge in 5G Networks With Context-Awareness," *IEEE Access*, pp. 8019–8034, 2016.
- [10] R. E. Rezagah, H. Shimodaira, G. K. Tran, K. Sakaguchi, and S. Nanba, "Cell discovery in 5G HetNets using location-based cell selection," in *IEEE Conf. Std. of Comm. & Netw.*, pp. 137–142, Oct. 2015.

- [11] G. C. Alexandropoulos, "Position aided beam alignment for millimeter wave backhaul systems with large phased arrays," in *IEEE Int. Workshop on Comput. Adv. in Multi-Sensor Adaptive Process.*, pp. 1–5, Dec. 2017.
- [12] M. Giordani, M. Mezzavilla, C. N. Barati, S. Rangan, and M. Zorzi, "Comparative analysis of initial access techniques in 5G mmWave cellular networks," in *Proc. Conf. Info. Science & Syst.*, 2016.
- [13] S. Habib, S. A. Hassan, A. A. Nasir, and H. Mehrpouyan, "Millimeter wave cell search for initial access: Analysis, design, and implementation," in *Int. Wireless Comm. and Mobile Comput. Conf.*, 2017.
- [14] J. Mo, P. Schniter, N. G. Prelcic, and R. W. Heath, "Channel estimation in millimeter wave MIMO systems with one-bit quantization," in *Proc. Asilomar Conf. Signals Syst. Comput.*, Nov. 2014.
- [15] J. Lee, G. Gil, and Y. H. Lee, "Channel Estimation via Orthogonal Matching Pursuit for Hybrid MIMO Systems in Millimeter Wave Communications," *IEEE Trans. Commun.*, 2016.
- [16] E. J. Candes and M. B. Wakin, "An Introduction to Compressive Sampling," *IEEE Signal Proc. Mag.*, 2008.
- [17] S. Li and G. Ge, "Deterministic Sensing Matrices Arising From Near Orthogonal Systems," *IEEE Trans. Info. Theory*, 2014.
- [18] J. A. Tropp, "Greed is good: algorithmic results for sparse approximation," *IEEE Trans. Info. Theory*, Oct. 2004.
- [19] N. Rajamohan, A. Joshi, and A. P. Kannu, "Joint Block Sparse Signal Recovery Problem and Applications in LTE Cell Search," *IEEE Trans. Veh. Tech.*, Feb. 2017.
- [20] S. Sun, G. R. MacCartney, and T. S. Rappaport, "A novel millimeter-wave channel simulator and applications for 5G wireless communications," in *Proc. IEEE Int. Conf. Commun.*, pp. 1–7, May 2017.
- [21] T. S. Rappaport, S. Sun, and M. Shafi, "Investigation and Comparison of 3GPP and NYUSIM Channel Models for 5G Wireless Communications," in *Proc. IEEE Veh. Tech. Conf.*, pp. 1–5, 2017.
- [22] M. A. and A. P. Kannu, "Channel Estimation Strategies for Multi-User mm Wave Systems," *IEEE Trans. Commun.*, Nov. 2018.
- [23] A. Jain, P. Sarvepalli, S. Bhashyam, and A. P. Kannu, "Change detection with sparse signals using quantum designs," *arXiv preprint arXiv:1901.08352*, 2019.
- [24] R. Baraniuk, M. Davenport, R. DeVore, and M. Wakin, "A Simple Proof of the Restricted Isometry Property for Random Matrices," *Constructive Approximation*, vol. 28, pp. 253–263, Dec. 2008.
- [25] H. Ghauch, T. Kim, M. Bengtsson, and M. Skoglund, "Subspace Estimation and Decomposition for Large Millimeter-Wave MIMO Systems," *IEEE J. Sel. Topics Signal Process.*, vol. 10, no. 3, pp. 528–542, 2016.
- [26] R. A. Horn and C. R. Johnson, *Matrix Analysis*. Cambridge University Press, New York, USA, 2nd ed., 2012.